International Journal of Innovative Research and Advanced Studies (IJIRAS)
Volume 13 Issue 6, June 2026

ISSN: 2394-4404

# Design And Development Of A Morphobot

**Tejesh S**

Assistant Professor, Department of Mechanical Engineering
Dr. Ambedkar Institute of Technology, Bengaluru, Karnataka, India

***Abstract:*** ***This project was undertaken to design and develop an Morphobot capable of operating in both ground and aerial environments with a controlled transition between the two modes. The system concept was based on integrating a terrestrial mobility mechanism and a vertical takeoff and landing aerial module within a single compact robotic platform. The primary objective was to achieve reliable ground navigation, stable transition, and sustained aerial flight while maintaining mechanical simplicity, structural integrity, and basic control stability suitable for a prototype-level implementation.***

***The overall system architecture, mechanical structure, propulsion components, and control hardware were designed and fabricated, and initial testing was performed on individual subsystems. Ground locomotion design and corrections were done on traction loss, uneven mass distribution, and limited torque availability under load conditions. Transition from ground to flight were designed based on center-of-gravity shifts, actuator interaction effects, and damping effect. Multiple aerial testing were conducted considering thrust-to-weight ratio, vibration-induced sensor noise, and control parameter tuning.***

***Keywords: Robot, Vertical take off, thrust, vibration, sensors, traction, torque.***



## I. INTRODUCTION

The working of Morphobot is based on a transformation mechanism that allows a single set of components to serve both flight and ground locomotion. Typically, the robot takes off and operates as a quadcopter or similar multirotor vehicle. Upon reaching the ground, servo motors rotate the arms or reconfigure the structure to allow the robot to rest or move on land. Flight is controlled by a flight controller using gyroscopic stabilization, while the transformation and ground mode are handled by microcontrollers coordinating the servo systems. The design ensures that the center of gravity remains stable in both configurations, and minimal additional components are used to keep the system lightweight and power efficient.

These designs use folding arms or wings that retract or collapse post-landing. The transformation is often powered by micro linear actuators or geared motors. These hybrid systems include wheels attached to the main frame, allowing the drone to roll on surfaces after landing. Some models use separate motors for ground propulsion, while others tilt their rotors for dual- mode actuation. Wheeled drones are particularly effective on flat surfaces and offer high efficiency in ground mode. This is suitable for high-speed flight but involves more complex mechanisms and structural constraints.

The main objective of the work is to develop a vehicle capable of seamlessly transitioning between aerial and terrestrial modes to navigate diverse environment efficiently.

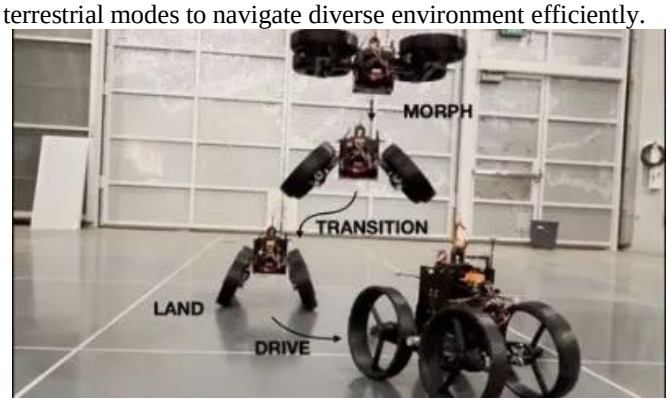


*Figure 1: Aerially transforming Morphobot*

ISSN: 2394-4404

## II. SCOPE OF THE WORK AND METHODOLOGY

### A. SCOPE OF THE WORK

The scope of the Morphobot work encompasses the design, development, and testing of a hybrid mobility system capable of both aerial and terrestrial movement. The primary objective is to create a vehicle that seamlessly transitions between flight and ground travel by integrating a dual-mode propulsion system. Lithium-polymer (LiPo) batteries will be employed for aerial operations, providing high energy density and reliable power, while solar energy will be harnessed for terrestrial movement, promoting sustainability and extended operational duration. The vehicle's structure will incorporate lightweight composite materials, such as carbon fiber-reinforced polymers (CFRP), to maintain a high strength-to-weight ratio. Autonomous control will be achieved through advanced navigation algorithms and real-time data integration from sensors like IMUs and GPS. The project will involve prototyping and rigorous testing to validate the vehicle's stability, power efficiency, and operational effectiveness. Applications will focus on areas such as environmental monitoring, disaster management, and remote surveillance, offering a versatile and energy-efficient solution for modern mobility challenges.

### B. METHODOLOGY

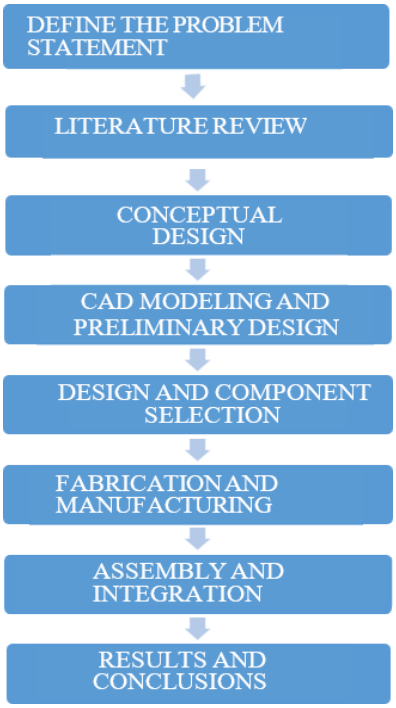


## III. DESIGN AND CALCULATIONS

### A. CALCULATIONS

Total mass of system 'm' = 1.6 kg
Gravitational acceleration 'g' = 9.81 m $s^{-2}$
Total weight W = m g
W = 1.6 × 9.81 W = 15.7 N
Thrust-to-weight ratio T / W = 2
Number of rotors n = 4
Motor-to-motor diagonal distance D = 450 mm = 0.45 m Arm length (frame center to motor center) L = D / 2 = 0.225 m Material (frame and arms) PETG
Top and bottom plate thickness t = 4 mm
Ground speed v = 0.37 m $s^{-1}$

### B. TOTAL THRUST CALCULATION

Total thrust required, T□ = 2 W
T□ = 2 × 15.7
T□ = 31.4 N
Thrust per motor T□ = T□ / n
T□ = 31.4 / 4 T□ = 7.85 N

### C. ARM ROOT BENDING MOMENT

Each arm is modeled as a cantilever beam subjected to an upward force at its free end.
Bending moment at the fixed end, M = T□ L
M = 7.85 × 0.225
M = 1.77 N·m

### D. MATERIAL PROPERTIES (PETG)

Young's modulus, E = 2.1 × $10^9$ N $m^{-2}$
Ultimate tensile strength, $\sigma_u \approx 45$ MPa
Factor of safety, FoS = 2.5
Allowable bending stress, $\sigma_a = \sigma_u$ / FoS
$\sigma_a = 45 / 2.5$ $\sigma_a = 18$ MPa

### E. ARM CROSS-SECTION PROPERTIES

Assumed rectangular cross-section:
Width, b = 20 mm = 0.02 m
Height, h = 10 mm = 0.01 m
Second moment of area, I = (b $h^3$) / 12
I = (0.02 × $0.01^3$) / 12
I = 1.67 × $10^{-9}$ m
Distance from neutral axis, y = h / 2
y = 0.005 m

### F. ARM BENDING STRESS

Maximum bending stress, σ = (M y) / I
σ = (1.77 × 0.005) / (1.67 × $10^{-9}$)
σ = 5.3 MPa
Safety check, σ < $\sigma_a$
5.3 MPa < 18 MPa.
Hence, the arm is structurally safe in bending.

### G. ARM DEFLECTION

Deflection at free end of a cantilever beam,
δ = (T□ $L^3$) / (3 E I)
δ = [7.85 × $(0.225)^3$] / [3 × 2.1 × $10^9$ × 1.67 × $10^{-9}$]
δ = 8.3 mm

ISSN: 2394-4404

This value is within acceptable limits for PETG UAV structures.

H. FOLDING ARM HINGE LOAD

Vertical shear force transmitted through hinge,
F□ = T□ F□ = 7.85 N
Design hinge load with safety factor,
F□,design = FoS × F□
F□,design = 2.5 × 7.85
F□,design = 19.6 N

I. MOTOR-INDUCED TORSIONAL LOAD

Motor rotational speed, $\omega = (2\pi N) / 60$
$\omega = (2\pi \times 25530) / 60$
$\omega = 2673$ rad $s^{-1}$
Assuming motor power, P =120 W
Motor torque, $\tau = P / \omega$
$\tau = 120 / 2673$
$\tau = 0.045$ N·m

J. LANDING IMPACT LOAD

Assumed vertical landing velocity, $v_{□} = 0.5$ m $s^{-1}$
Landing gear compression, s = 0.01 m
Impact force, $F_i = (m\ v_{□}^2) / (2\ s)$
$F_i = (1.6 \times 0.25) / 0.02$
$F_i = 20$ N
Design landing load (with safety factor ≈ 2),
$F_{i,design} = 40$ N
Load per landing leg, $F_{□} = F_{i,design} / 4$
F□ = 10 N

K. GROUND STATIC LOAD (WHEELS)

Static load per wheel, $F_v = W / 4$
$F_v = 15.7 / 4$
$F_v = 3.9$ N

L. GROUND BRAKING LOAD

Assumed stopping time, t = 0.2 s
Deceleration, a = v / t
a = 0.37 / 0.2
a = 1.85 m $s^{-2}$
Braking force, $F_\beta = m\ a$
$F_\beta = 1.6 \times 1.85$
$F_\beta = 3.0$

M. MOTOR SPEED CALCULATION

RPM = *KV * V*
RPM = 2300 × 11.1 = 25,530 RPM
n=25530/60 = 425.5 rev/s

N. TOTAL THRUST FOR A QUAD CONFIGURATION

$T_{Total} = 4 \times T_{Motor}$
$T_{Total} = 4 \times 560 = 2240$ g (2.24 kg)

O. BATTERY SELECTION AND FLIGHT TIME

Battery: 3S Li-Po(11.1 V, 2200 Mah = 2.2Ah)
Usable capacity (80 %) = 1.76 Ah
Estimated flight time: 3–5 minutes (typical for 2200 Mah 3S quad setup)

## IV. MODELLING USING VISSION 360

A. TOP PLATE

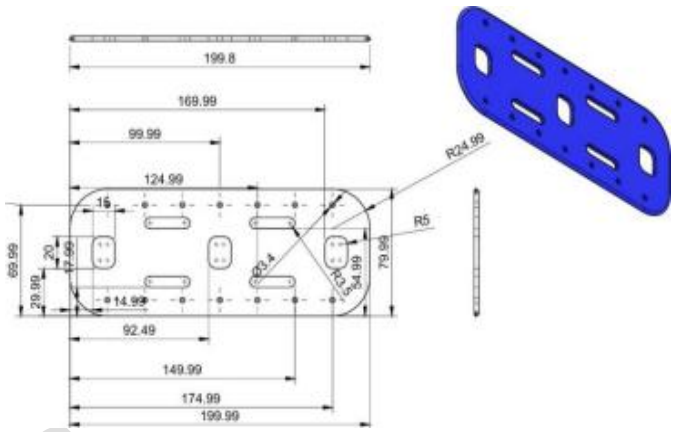


*Figure 2: 2D drawing of top plate*

B. BASE PLATE

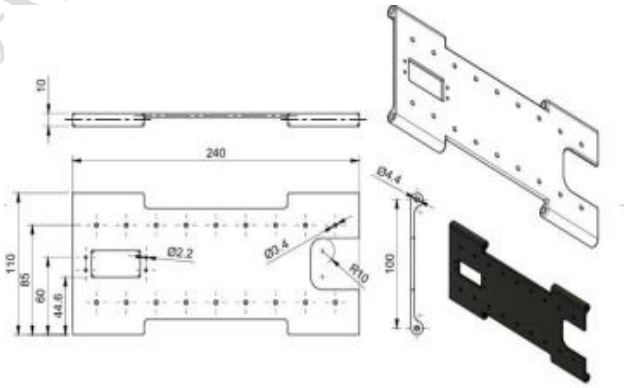


*Figure 3: 2D drawing of base plate*

C. ARMS

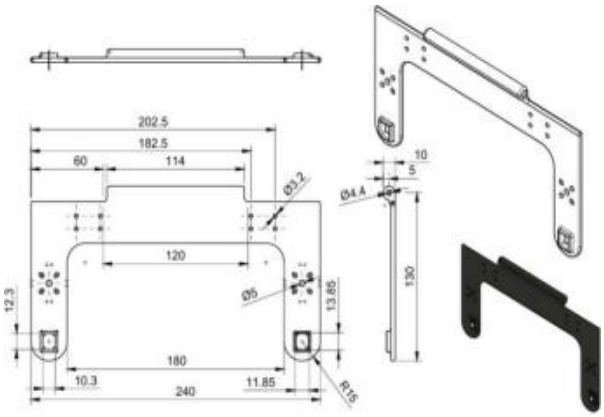


*Figure 4: 2D drawing of arms*

D. MODEL

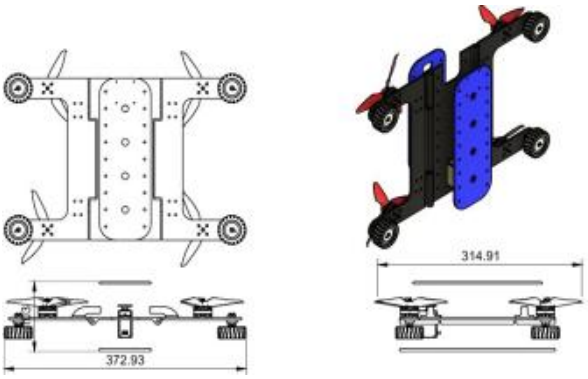


*Figure 5: 2D drawing of the model*

E. 3D MODEL OF THE MORPHOBOT FRAME

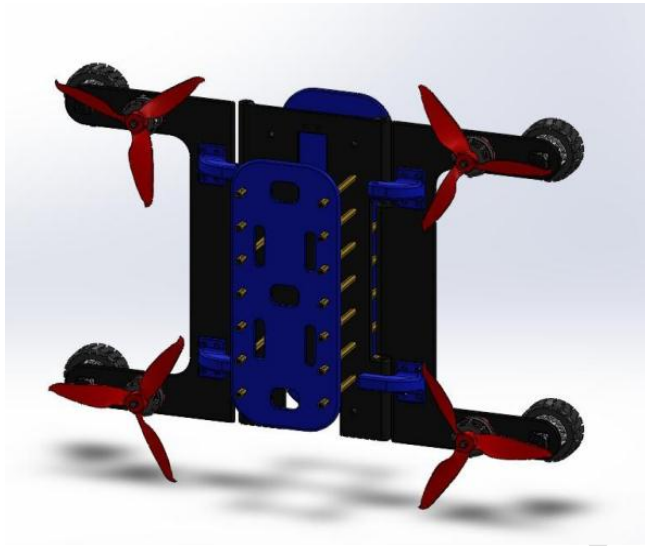

*Figure 6: Isometric view of the frame*

## V. FABRICATION

### A. MATERIALS USED

Two primary thermoplastic materials were employed for the robot's fabrication: PLA

(Polylactic Acid) and PETG (Polyethylene Terephthalate Glycol-Modified).

- ✓ PETG was used for the main load-bearing components, namely the arms and central plate, which require enhanced toughness and impact resistance.
- ✓ PLA was used for non-load-bearing parts such as hooks and external fixtures, where lightweight and dimensional accuracy are prioritized.

### B. MATERIAL DESCRIPTION

| Property | PLA | PETG |
|---|---|---|
| Density (g/cm³) | 1.25 | 1.27 |
| Tensile Strength (MPa) | 60 | 55 |
| Elongation at Break (%) | 4–6 (brittle) | 20–25 (ductile) |
| Glass Transition Temperature (°C) | 60 | 80 |
| Melting Temperature (°C) | 180–220 | 230–250 |
| Strength-to-Weight Ratio (MPa·cm³/g) | 48 | 43 |
| Impact Resistance | Low | High |
| Printability | Very easy | Moderate |
| Moisture Sensitivity | Low | Moderate |

*Table 1: Material Properties*

### C. PRINTING PROCESS

The components were fabricated using the FDM process with the following steps:

- ✓ CAD Modeling: All parts were designed in SolidWorks according to structural and dimensional requirements.
- ✓ Slicing: The models were sliced into 0.2 mm layers using Cura software to generate G- code for the printer.
- ✓ Material Deposition: The extruder nozzle, heated to 200–240 °C depending on the filament, deposited molten material layer-by-layer on a heated bed.
- ✓ Cooling and Solidification: Each layer cooled and fused with the previous one to form a rigid part.
- ✓ Post-Processing: Minor supports were removed and the parts were inspected for dimensional accuracy before assembly.

### D. MATERIAL APPLICATION

PETG for Arms and Main Plate -The arms and central plate form the primary load-bearing structure of the Aero-Terrestrial Robot. These parts experience mechanical stresses, vibrations, and impact loads during both aerial flight and ground movement.

Advantages of PETG for Structural Components:

- ✓ High Impact Strength: PETG offers superior toughness and flexibility compared to PLA, allowing it to absorb shocks during landings and transitions between aerial and terrestrial modes.
- ✓ Improved Layer Adhesion: PETG bonds strongly between layers, reducing delamination under load and enhancing durability.
- ✓ Higher Thermal Resistance: The higher glass transition temperature (~80 °C) prevents softening under motor heat or sunlight exposure.
- ✓ Balanced Strength-to-Weight Ratio: With a tensile strength of approximately 55 MPa and density of 1.27 g/cm³, PETG provides an excellent strength-to-weight ratio (~43 MPa·cm³/g), ensuring robust yet lightweight structural performance.
- ✓ Moderate Flexibility: The 20–25% elongation at break allows the arms to flex slightly under stress without fracturing — a critical property during rough landings or impacts.

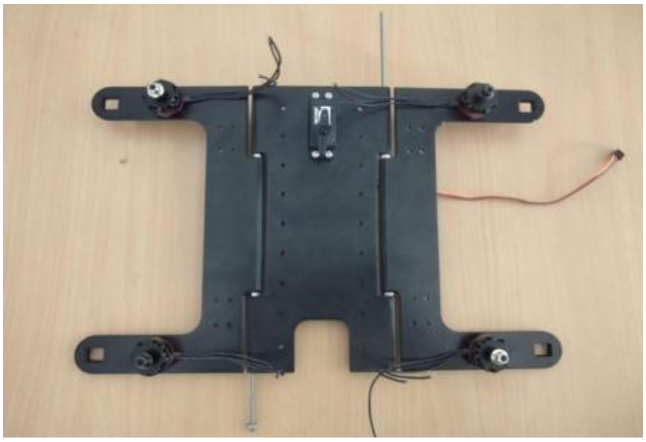

*Figure 7: PETG for Arms & Main plate*

E. PLA FOR HOOKS AND SECONDARY FIXTURES

PLA was used for non-critical elements such as hooks, covers, and fittings due to its light weight, ease of printing, and excellent dimensional precision. PLA's higher rigidity and smooth surface finish help achieve accurate and stable attachment mechanisms without adding unnecessary structures.

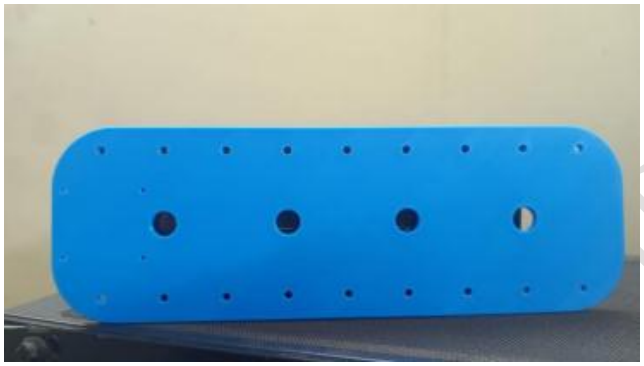

*Figure 8: PLA mounts for electronic components*

F. SUMMARY OF MATERIAL UTILIZATION

| Components | Material | Key Benefit |
|---|---|---|
| Arms | PETG | High impact strength and flexibility; |
| Main Plate | PETG | Excellent structural |
| Hooks & Fixtures | PLA | Lightweight, rigid, easy to fabricate |

*Table 2: Materials used*

## VI. CONCLUSION

This overall work presents the design and development of an Morphobot system, addressing the challenges of combining aerial and ground mobility within a single platform. The work successfully establishes a clear system architecture, supported by informed component selection, mechanical design, and subsystem-level implementation. Preliminary testing of actuators, structural elements, and control hardware confirms that the proposed design is technically feasible and capable of supporting both operational modes at a conceptual level.

Future work will concentrate on complete hardware–software integration, closed-loop control tuning, and extensive ground and flight testing to ensure stable transitions between aerial and terrestrial modes. Additional improvements such as weight optimization, enhanced sensor fusion, and advanced control strategies will further improve reliability and autonomy. With systematic refinement and dedicated testing, the proposed system has strong potential to mature into a robust, scalable Morphobot platform suitable for research and real-world deployment.

## REFERENCES

[1] J. Mulgaonkar, G. Cross, and V. Kumar, "Design and development of a wheeled quadcopter," Proceedings of the IEEE International Conference on Robotics and Automation (ICRA), 2016.
[2] R. J. Full, D. E. Koditschek, and P. Holmes, "Biologically inspired multi-modal locomotion," Science Robotics, vol. 2, 2017.
[3] A. Kalantari and M. Spenko, "Design and control of a transformable aerial–ground robot," IEEE Transactions on Robotics, vol. 34, 2018.
[4] J. Lee, H. Kim, and S. Park, "Energy management strategies for hybrid aerial– terrestrial robots," IEEE Robotics and Automation Letters, vol. 4, 2019.
[5] R. Kumar, S. Mishra, and P. Verma, "Material selection and lightweight design considerations for hybrid robotic systems," Materials Today: Proceedings, vol. 18, pp. 4567–4574, 2019.[6] Z. Wang, Y. Chen, and L. Zhang, "Sensor fusion and perception for hybrid aerial–ground robots," Sensors, vol. 20, 2020.
[6] M. Saska, T. Baca, J. Thomas, and L. Preucil, "Hybrid aerial–ground robotic
[7] systems for inspection tasks," IEEE Robotics & Automation Magazine, vol. 23, 2016.
[8] N. Michael, J. Fink, and V. Kumar, "Cooperative hybrid robots for multi- environment operation," Autonomous Robots, vol. 41, 2017.
[9] Pounds, R. Mahony, and P. Corke, "Rolling and flying robots: Energy-efficient mobility strategies," Journal of Field Robotics, vol. 34, no. 2, 2017.
[10] S. Mintchev, S. de Rivaz, and D. Floreano, "Bio-inspired multimodal locomotion in hybrid robots," Bioinspiration & Biomimetics, vol. 13, 2018.
A. Kalantari and M. Spenko, "Design trade-offs in hybrid ground–air robots," IEEE Transactions on Mechatronics, vol. 23, 2018.
[11] Floreano, M. Mintchev, and S. Scaramuzza, "Autonomous hybrid robots for exploration," Nature Robotics, vol. 3, 2018.
[12] T. Toksoz, M. Unal, and K. Erdem, "Hybrid robots for confined-space navigation," Robotics and Autonomous Systems, vol. 117, 2019.
[13] X. Chen, Y. Liu, and Z. Sun, "Lightweight materials and structures for hybrid robots," Composite Structures, vol. 234, 2020.

ISSN: 2394-4404

[14] Patel, S. Shah, and A. Mehta, "Autonomous decision-making in hybrid ground– air robots," IEEE Robotics and Automation Letters, vol. 5, 2020.
[15] L. Rossi, F. Bianchi, and M. Ferri, "Fault-tolerant design of aero-terrestrial robots," Robotics, vol. 9, 2020.
[16] Huang, J. Wu, and Y. Lin, "Vision-based terrain classification for hybrid robotic systems," Sensors, vol. 21, 2021.
[17] T. Nguyen, A. Pham, and D. Tran, "Hybrid aero-terrestrial robots for agricultural monitoring," Computers and Electronics in Agriculture, vol. 182, 2021.
[18] P. Sharma, R. Singh, and V. K. Jain, "A survey on aero-terrestrial robotic systems," IEEE Access, vol. 10, 2022.
[19] Bogue, "Hybrid ground–air robots for infrastructure inspection," Industrial Robot: The International Journal of Robotics Research and Application, vol. 49, 2022